M&C 2017 - International Conference on Mathematics & Computational Methods Applied to Nuclear Science & Engineering, Jeju, Korea, April 16-20, 2017, on USB (2017)

Neutron and Gamma-ray Energy Reconstruction for Characterization of Special Nuclear Material

S. D. Clarke*, M. C. Hamel, A. Di Fulvio, S. A. Pozzi

Department of Nuclear Engineering and Radiological Sciences, University of Michigan, Ann Arbor, MI 48109
**clarkesd@umich.edu*

Abstract – *Characterization of special nuclear material may be performed using energy spectroscopy of either the neutron or gamma-ray emissions from the sample. Gamma-ray spectroscopy can be performed relatively easily using high-resolution semiconductors such as high-purity germanium. Neutron spectroscopy, on the other hand, is a complex inverse problem. Here, results are presented for ^{252}Cf and PuBe energy spectra unfolded using a single EJ309 organic scintillator; excellent agreement is observed with the reference spectra. Neutron energy spectroscopy is also possible using a two-plane detector array, whereby time-of-flight kinematics can be employed. With this system, energy spectra can also be obtained as a function of position. Spatial-dependent energy spectra are presented for neutron and gamma-ray sources that are in excellent agreement with expectations.*

I. INTRODUCTION

Energy spectroscopy is useful for characterizing special nuclear material (SNM). Isotope-specific gamma rays are emitted at specific energies, which allows for very accurate determination of the SNM composition. Semiconductors and inorganic scintillators are the most commonly employed detectors for these applications.

Neutron spectroscopy, on the other hand, is a much more difficult task. The response of organic scintillators is related to the incident neutron energy; however, neutrons interact in organic scintillators though elastic scattering, which creates a weak coupling between the measured detector response and the energy spectrum of the incident neutrons.

If there are multiple sources in field-of-view of the detector, imaging techniques can be employed to isolate the location of the individual sources. Once the location of the sources is determined, the energy spectrum of the incident particles may be extracted for any region in the field-of-view using the coincident scatter data from the imager.

Here we present neutron energy spectrum unfolding results from a single EJ-309 liquid scintillator. In addition, we present spatial-dependent energy spectra using our dual-particle imaging array of EJ-309 and NaI(Tl) scintillators.

II. NEUTRON ENERGY SPECTRUM UNFOLDING

Neutron energy spectra can be derived by unfolding the detector response from the detected pulse height spectrum. In general, the unfolding problem can be defined as Eq. 1 below.

$$z_{0i} + e_i = \sum_{j=1}^{M} R_{ij}\Phi_j \tag{1}$$

z_{0i} is the light output in the i^{th} bin
e_i is the error associated with the i^{th} light output bin
M is the number of detection channels
$R_{ij}(E)$ is the detector response element for the i^{th} light output bin, and the j^{th} neutron energy bin
$\Phi_j(E)$ Neutron spectrum flux cm^{-2}, in the j^{th} energy bin

1. Solution Methodology

One approach to solving Eq. 1 is direct inversion the response matrix. The matrix itself can be obtained by simulating monoenergetic neutrons in the energy range of interest, using a Monte Carlo code such as MCNPX-PoliMi and MPPost [1–3]. Due to the ill-conditioning of the response matrix, the direct-inversion approach typically yields an oscillatory solution for the incident energy spectrum; this solution is not stable with respect to the uncertainty of the measured data. The statistical fluctuations and the amplitude of the oscillations can be as large as the estimated values themselves.

To overcome this issue, regularization is often applied. One type of regularization function is based on the spectral entropy. It can be shown that the entropy is a measurement of the smoothness of a histogram [4]. Applying a regularization function consists in imposing a smoothing condition to the estimate of the flux histogram. A regularization function, as in Eq. 2, is obtained using a Bayesian approach, which incorporates the prior information.

$$H(y) = -\sum_{i=1}^{M} p_i \log p_i \tag{2}$$

$H(\boldsymbol{y})$ is the entropy of a probability distribution $\boldsymbol{p} = (p_1 \ldots p_n)$; the values to be estimated, $\boldsymbol{y}$, are random variables. According to Bayes theorem, the joint probability density function, $f(\boldsymbol{y} \mid \boldsymbol{z})$, depends on $L(\boldsymbol{z} \mid \boldsymbol{y})$, as in Eq. 3. $L(\boldsymbol{z} \mid \boldsymbol{y})$ is the likelihood function, i.e. the conditional probability for the data $\boldsymbol{z}$, given $\boldsymbol{y}$ and the *apriori* information $ph(\boldsymbol{y})$.

$$f(y \mid z) \propto L(z \mid y)ph(y) \tag{3}$$

One wants to find $\hat{y}$ that maximizes $f(\boldsymbol{y} \mid \boldsymbol{z})$, or its logarithm. In absence of any other *apriori* information, the probability density function $f(\boldsymbol{y} \mid \boldsymbol{z})$ of a certain histogram is proportional to the number of possible combinations of the data in the bins, i.e. the entropy of the data.

2. Results

We evaluated ^{252}Cf and PuBe neutron spectra obtained using the MAXED code, a Bayesian algorithm based on entropy maximization [5]. This method translates prior knowledge available about the problem (such as spectra positivity and energy boundaries) into a prior model, which is coupled with the observation model (or likelihood) to derive the posterior distribution of the unknown neutron spectra.

Experimental data were collected for comparison. One 7.62 cm diameter by 7.62 cm length EJ-309 detector was irradiated with two sources: ^{252}Cf (~25 μCi) and PuBe (1 Ci) to evaluate its performance as neutron spectrometer. Source-to-detector distance was 1.5 m for ^{252}Cf and 1 m for PuBe. Prior to neutron irradiation, the detector was calibrated using a ^{137}Cs source, to match 80% of the Compton edge peak (478 keVee) to a pulse amplitude of 0.3 V. The neutron spectrum was separated from the photon spectrum using a pulse shape discrimination algorithm, based on charge integration [6].

Figures 1 and 2 show the unfolded spectra from ^{252}Cf and PuBe sources. In Fig. 1, the peak in the unfolded spectrum appears at higher energies than the reference due the detection threshold. Given that, we consider the unfolded spectra in satisfactory agreement with the reference spectra, i.e. the analytic model by Mannhart [7] for spontaneous fission ^{252}Cf source and the measured one for (alpha, n) PuBe source [8]. A low energy limit of about 400 keV and 1 MeV was achieved for PuBe and ^{252}Cf, respectively. Although the simulated response matrix extends below 100 keV, the practical unfolding limit at low energies is a few hundred keV because of uncertainties in the light output function and fidelity of the pulse shape discrimination. The ^{252}Cf spectrum was unfolded using a flat guess spectrum, conversely the reference spectrum was incorporated as prior information, to unfold the PuBe data. Ill-conditioning of the EJ-309 response matrix and the smoothing entropy maximization did not allow to resolve the peaks in the spectrum, due to the excited states of ^{12}C (^{9}Be(alpha,n)^{12}C*), when a flat guess spectrum was used.

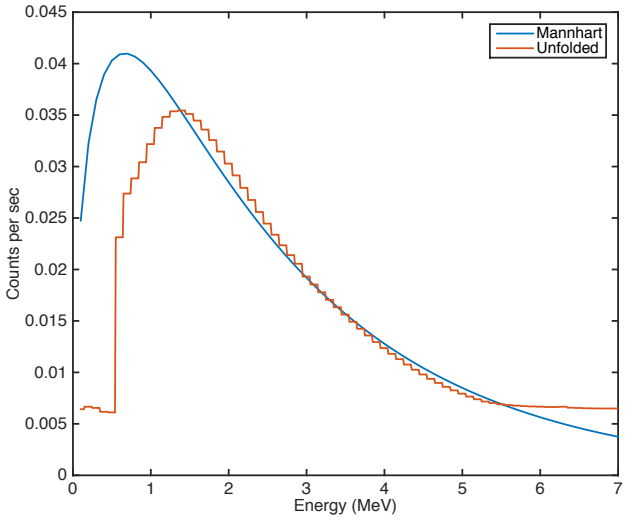

Fig. 1. Unfolded neutron energy spectrum from ^{252}Cf detected with an EJ-309 liquid scintillator; the Watt spectrum from Mannhart [7] is shown for reference.

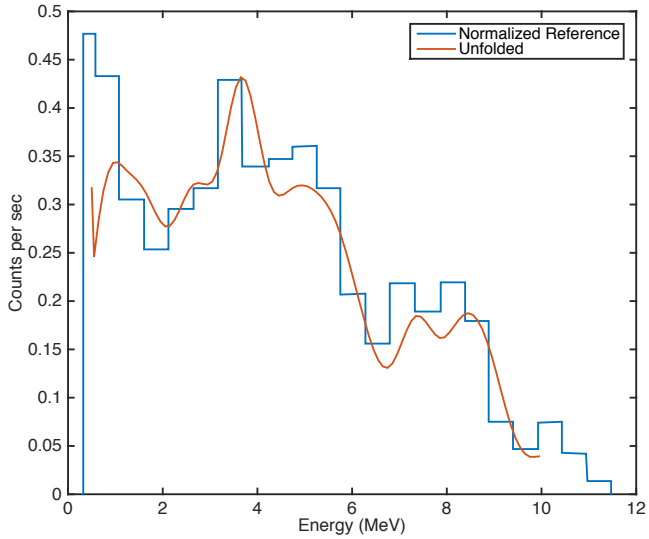

Fig. 2. Unfolded neutron energy spectrum from PuBe detected with an EJ-309 liquid scintillator; a normalized PuBe spectrum from Knoll [8] is shown for reference.

III. SPATIAL-DEPENDANT ENERGY SPECTRA

The dual-particle imager (DPI) is a combined Compton and neutron scatter camera that is sensitive to both neutrons and gamma-rays [9, 10]. The system works as an imager and spectrometer for both particle types. The system is configured in two-planes and uses liquid organic and NaI(Tl) scintillators. The pulse shape discrimination capabilities and fast response of the liquid scintillators makes them well suited for this system.

Image reconstruction was performed on the data using the stochastic origin ensembles (SOE) method. This method

uses Markov chain Monte Carlo to iteratively construct an image with improved signal-to-noise ratio and resolution compared to backprojection imaging [11]. The incident energy is obtained for both neutrons, by using time-of-flight, and gamma-rays by summing both energy depositions. Spectra are isolated by using the SOE algorithm to create separate images binned by energy. The intensity of a particular pixel can then be translated from each energy binned image to an energy spectrum. To maintain adequate statistics while progressing through the Markov chain, the energy binned images are summed during each iteration for the acceptance or rejection of re-sampled event origins.

The DPI was used for an experiment with a ^{252}Cf and ^{60}Co source. The ^{252}Cf, which emits both neutrons and gamma-rays, was placed at an angular location of (114° azimuth, 93° inclination) at 175 cm. It had an activity of 3.3×10^4 fissions per second. The ^{60}Co had coordinates of (55°, 85°) and was located 390 cm from the DPI. For reference, the coordinates for a source directly centered on the face of the DPI would be (90°, 90°). The ^{60}Co had an activity of 63 μCi.

The neutron image, in Fig. 3, locates the ^{252}Cf with a hot-spot. The ^{60}Co source is not seen because it emits only gamma-rays. However, in the reconstructed gamma-ray image (Fig. 4), the ^{60}Co source produces a distinct hot-spot. The hot-spot from the ^{252}Cf gamma-rays is very faint and blends into the background. In this experiment both point sources are significantly smaller than a single image pixel; therefore, the reconstructed image is as expected.

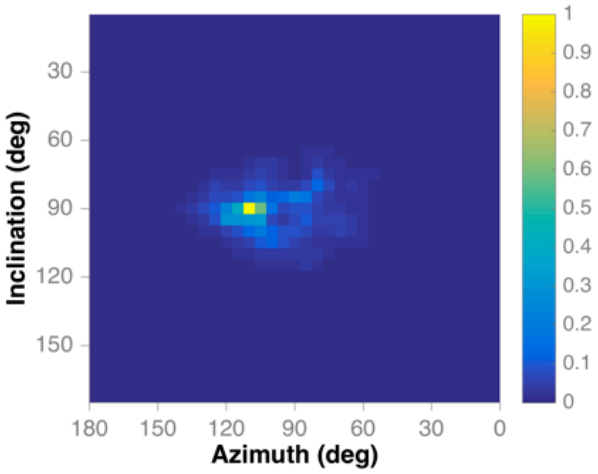

Fig. 3. Neutron image reconstructed using SOE

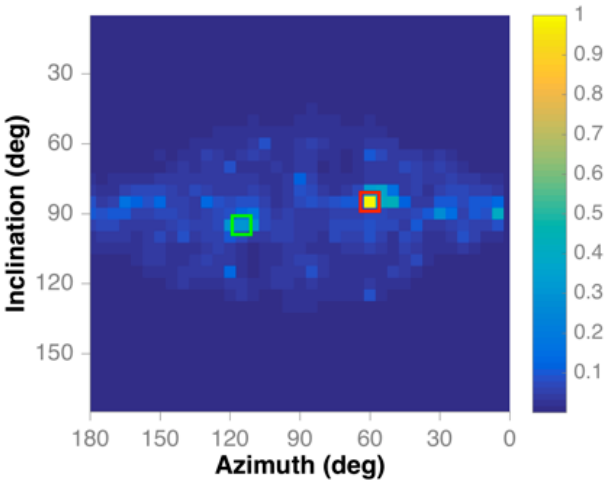

Fig. 4. Photon image reconstructed using SOE.

Figure 5 show the reconstructed energy spectrum of the neutrons imaged in Fig. 3, which only the 252Cf neutron spectrum in this case; if there were other neutron enitters in the field-of-view their spectra would be reconstructed as well. In the gamma-ray case, spectrum isolation is very useful because we can take a localized gamma-ray spectrum from the location of neutron hot-spot. These localized spectra were isolated from the ^{60}Co and ^{252}Cf hot-spots as well as a pixel containing environmental background (85°, 115°). Figure 6 clearly shows a distinction between all three spectra. The ^{60}Co has the two expected peaks at 1.17 and 1.33 MeV while the ^{252}Cf spectrum has the shape of a spectrum from fission gamma-rays. The background pixel has a much lower count rate than the other two and a different spectral shape as well.

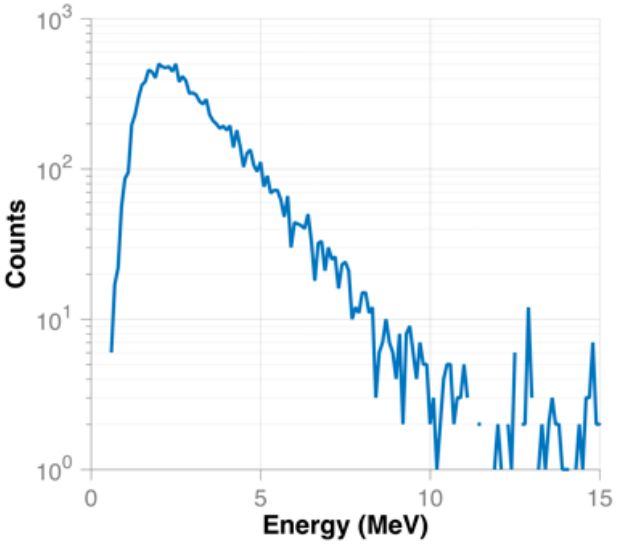

Fig. 5. Reconstructed neutron energy spectrum at the position shown in Fig. 3.

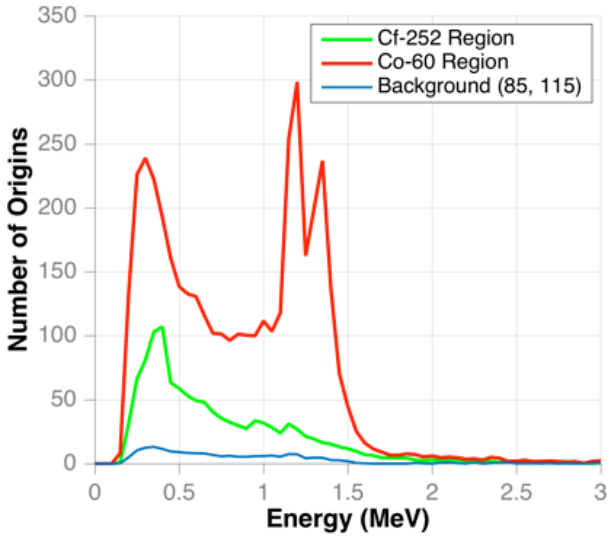

Fig. 6. Reconstructed gamma-ray energy spectra at the positions shown in Fig. 4.

IV. CONCLUSIONS

We have presented effective neutron energy reconstruction using a single EJ-309 liquid scintillator as well as spatial-dependent neutron and gamma-ray energy reconstruction using an array of EJ-309 and NaI(Tl) scintillators. The results shown here illustrate that the reconstruction from the single detector is applicable to discriminating fission from (alpha, n) sources, for example metal versus oxide forms of SNM. In the presence of multiple sources, the DPI can be employed to isolate energy spectra to a specific region in space.

REFERENCES

1. S. A. POZZI, et al., "MCNPX-PoliMi for Nuclear Nonproliferation Applications," *Nucl. Instr. Meth. A*, **694**, 119 (2012).
2. E. C. MILLER et al., "MCNPX-PoliMi Post-Processing Algorithm for Detector Response Simulations," *Jour. Nucl. Mater. Management*, **XL(2),** 34 (2012)
3. A. ENQVIST, et al., "Neutron Light Output Response and Resolution Functions in EJ-309 Liquid Scintillation Detectors," *Nucl. Instr. Meth. A*, **715**, 79 (2013).
4. G. COWAN, Statistical Data Analysis, Oxford Science Publications, ISBN-10 0198501552 (2000).
5. M. REGINATTO, et al., "Spectrum unfolding, sensitivity analysis and propagation of uncertainties with the maximum entropy deconvolution code MAXED," *Nucl. Instr. Meth. A*, **476,** 242 (2002).
6. J. K. POLACK, et al., "An Algorithm for Charge-Integration, Pulse-Shape Discrimination and Estimation of Neutron/Photon Misclassification in Organic Scintillators," *Nucl. Instr. Meth. A*, **795**, 253 (2015).
7. W. MANNHART, "Status of Cf-252 Neutron Spectrum as a Standard," React. Dosim. Methods," *Appl. Stand.*, 340 (1989).
8. G. KNOLL, "Radiation Detection and Measurement", 4th edition, Wiley (2010).
9. A. POITRASSON-RIVIERE, et al., "Dual-particle imaging system based on simultaneous detection of photon and neutron collision events," *Nucl. Instr. Meth. A,* **760**, 40 (2014).
10. A. POITRASSON-RIVIERE, et al., "Angular-resolution and material-characterization measurements for a dual-particle imaging system with mixed-oxide fuel," *Nucl. Instr. Meth. A*, **797**, 278 (2015).
11. M. C. HAMEL, et al., "Stochastic image reconstruction for a dual-particle imaging system," *Nucl. Instr. Meth. A*, **810**, 120 (2016).